Accepted Manuscript

Genesis of a giant Paleoproterozoic strata-bound magnesite deposit: constraints from Mg isotopes

Aiguo Dong, Xiang-kun Zhu, Shizhen Li, Brian Kendall, Yue Wang, Zhaofu Gao

PII: S0301-9268(16)30224-8
DOI: http://dx.doi.org/10.1016/j.precamres.2016.06.020
Reference: PRECAM 4541

To appear in: *Precambrian Research*

Received Date: 21 October 2015
Revised Date: 17 June 2016
Accepted Date: 18 June 2016

Please cite this article as: A. Dong, X-k. Zhu, S. Li, B. Kendall, Y. Wang, Z. Gao, Genesis of a giant Paleoproterozoic strata-bound magnesite deposit: constraints from Mg isotopes, *Precambrian Research* (2016), doi: http://dx.doi.org/10.1016/j.precamres.2016.06.020

Genesis of a giant Paleoproterozoic strata-bound magnesite deposit: constraints from Mg isotopes

Aiguo Dong[a], Xiang-kun Zhu[a*], Shizhen Li[a], Brian Kendall[b], Yue Wang[a], Zhaofu Gao[a]

[a] *MLR Laboratory of Isotope Geology, State Key Laboratory of Continental Dynamics, Institute of Geology, Chinese Academy of Geological Sciences, Beijing 100037, China.*

[b] *Department of Earth and Environmental Sciences, University of Waterloo, 200 University Avenue West, Waterloo, ON, N2L 3G1, Canada*

[*] Corresponding author.

E-mail addresses: xiangkun@cags.ac.cn (X-K, Zhu); aiguo.dong@cags.ac.cn (A Dong); bkendall@uwaterloo.ca (B Kendall)

ABSTRACT

Giant strata-bound magnesite deposits are absent in modern and most Phanerozoic sedimentary environments but occur predominantly in Precambrian strata. These deposits may have formed directly through precipitation of evolved Mg-rich seawater in an evaporative shallow-marine setting or, alternatively, by epigenetic-hydrothermal replacement of the Mg-rich carbonate precursor. To test these hypotheses, we obtained the first Mg isotope data from the world's largest strata-bound magnesite deposit belt, hosted by the ca. 2.1 Ga Dashiqiao Formation in Northeast China. The Mg isotope compositions (δ^{26}Mg) of most magnesite ores in the Huaziyu deposit are heavier (–0.75 ± 0.26‰) than most Proterozoic sedimentary dolomite. The Mg isotope compositions and

major and trace element data indicate that the magnesites are probably not of hydrothermal origin. Instead, a Mg-rich carbonate precursor precipitated from evaporating seawater in a semi-closed system. Diagenetic brines altered the Mg-rich carbonate precursor to magnesite. Subsequently, recrystallization during regional metamorphism produced coarsely crystalline and saddle magnesite. These interpretations are consistent with the geological features and other geochemical data (element concentrations and C and O isotopes) for the magnesite ores. Hence, we interpret the formation of the Huaziyu magnesite deposit to be dominated by evaporative sedimentation and brine diagenesis.

Keywords: Mg isotopes; magnesite deposit; Paleoproterozoic; evaporative sedimentation; diagenesis

1. Introduction

The world's largest strata-bound magnesite ($MgCO_3$) deposits, suggested to be of Veitsch-type magnesite (i.e., hosted by marine carbonates; Pohl, 1990), occur in Paleoproterozoic carbonates of the ca. 2.1 Ga Dashiqiao Formation of Northeast (NE) China (Zhang, 1988). Deposition of the magnesite ores occurred during the ca. 2.22-2.06 Ga Lomagundi Event, which marks a time of dramatic changes in Earth's surface environment (Bekker and Holland, 2012). The Lomagundi Event is associated with high rates of organic carbon burial (reflected by a worldwide positive $\delta^{13}C$ excursion in carbonates) and relatively high seawater sulfate concentrations (reflected by deposition of marine evaporites containing gypsum and anhydrite, as well as by the sulfur isotope

compositions of sedimentary sulfate and pyrite) that together point to an episode of increased atmosphere and ocean oxygenation (Bekker and Holland, 2012; Bekker et al., 2006; Melezhik et al., 2005; Planavsky et al., 2012; Reuschel et al., 2012; Schröder et al., 2008; Scott et al., 2014).

Deposition of the magnesite ores may suggest locally high seawater Mg/Ca ratios. Thin beds of magnesite can precipitate from Mg-rich seawater in modern saline lakes, playas, or sabkhas (Power et al., 2014), but large-scale strata-bound magnesite deposits occur mainly in Precambrian strata (Frank and Fielding, 2003). Precipitation of evolved Mg-rich seawater in an evaporative marine setting may have triggered the formation of giant strata-bound magnesite deposits (Pohl, 1990). However, an alternative hypothesis is that epigenetic-hydrothermal processes formed magnesite via the replacement of sedimentary carbonate rocks, with the Mg being derived from leaching of dolostones or other Mg-rich rocks in the region (Aharon, 1988; Henjes-Kunst et al., 2014).

Thus, new evidence is needed to resolve the controversy about the genesis of giant strata-bound magnesite deposits. These deposits are typically affected by greenschist to amphibolite facies metamorphism (Zhang, 1988). In contrast with traditional stable isotope tracers used to study magnesite deposits (e.g., C and O isotopes), Mg isotope fractionation is limited in bulk samples during prograde metamorphic dehydration and early diagenesis as inferred from similar Mg isotope compositions in greenschist to eclogite facies rocks from eastern China and carbonate sediments from Ocean Drilling Program site 807, respectively (Higgins and Schrag, 2012; Wang et al., 2014). Moreover, limited Mg isotope fractionation occurs during high-temperature igneous differentiation whereas pronounced isotope fractionation is observed during low-temperature geological

processes, such as chemical precipitation, dolomitization, and fluids metasomatism (Azmy et al., 2013; Galy et al., 2002; Geske et al., 2015a; Immenhauser et al., 2010; Lavoie et al., 2014; Shirokova et al., 2013; Teng et al., 2007; Walter et al., 2015). Hence, the Mg isotope composition of magnesite has potential to distinguish between competing hypotheses for the genesis of giant strata-bound magnesite deposits. We use Mg isotopes together with element concentrations and C and O isotopes to trace the metallogenic processes responsible for the formation of the giant strata-bound Huaziyu magnesite deposit hosted by the Dashiqiao Formation.

2. Geological setting

The North China Craton (NCC) is one of the oldest cratons on Earth and is endowed with a wealth of ore deposit types such as banded iron formations (BIFs), SEDEX Pb-Zn deposits, massive sulfide deposits, strata-bound magnesite deposits, and boron deposits (Zhao and Zhai, 2013). In the Liaohe Group of the NCC, dozens of strata-bound magnesite deposits are found in a belt 60 km long by 1-2 km wide that extends from the cities of Dashiqiao to Haicheng (Zhang, 1988) (Fig. 1a). These giant strata-bound magnesite deposits underwent greenschist to amphibolite facies regional metamorphism at ~1.9 Ga and had an intense recrystallization to form the coarsely crystalline and saddle magnesite (Zhao and Zhai, 2013).

Generally, the Liaohe Group is subdivided into five formations in the Dashiqiao area. In ascending stratigraphic order, these comprise the Langzishan Formation, Lieryu Formation, Gaojiayu Formation, Dashiqiao Formation, and Gaixian Formation (Zhang, 1988; Zhao and Zhai, 2013). The Dashiqiao Formation is dominated by carbonate rocks

and is subdivided into three Members (Zhang, 1988). The lowermost Member 1 comprises thin limestone interbedded with calcareous shale. Member 2 is characterized by shale intercalated with sandstone and limestone. The uppermost Member 3 is the thickest member and is dominated by dolomitic carbonates that host the strata-bound magnesite deposits, including the Huaziyu deposit. The magnesite deposits are stratiform and conformable with their host rocks. Along with the magnesite deposits, ca. 40-50 cm thick interlayers of lenticular sedimentary gypsum (Chen et al., 2002) and variously shaped stromatolites (Zhang, 1988) are found in the host rocks (Fig. 1b). Based on the rock and mineral assemblages and their geochemistry, a range of sedimentary facies are represented in the Dashiqiao Formation, including (from north to south) littoral clastic, restricted platform, littoral beach and bar, semi-restricted platform, and open platform facies (Chen et al., 2002; Dong et al., 1996; Feng et al., 1995). The magnesite-bearing Member 3 carbonates were likely deposited in a restricted platform setting such as a lagoon.

Zircons from a fine-grained biotite gneiss in the Lieryu Formation, stratigraphically below the Dashiqiao Formation, yielded a U-Pb age of 2179 ± 8 Ma that represents the crystallization age of the original volcanic rock and thus a maximum depositional age constraint for the Dashiqiao Formation (Wan et al., 2006). Detrital zircons from the Gaixian Formation, stratigraphically overlying the Dashiqiao Formation, yielded U-Pb ages from ca. 2225 to 2021 Ma (Wan et al., 2006). Hence, the Gaixian Formation must have been deposited after ca. 2021 Ma. Calcium sulfate minerals are found within the magnesite deposits (Chen et al., 2002), suggesting deposition of the host carbonate sediments during the Lomagundi Event (Bekker et al., 2006; Melezhik et al., 2005;

Planavsky et al., 2012; Reuschel et al., 2012; Schröder et al., 2008). Combined, these geochronological and geological constraints suggest that the Dashiqiao Formation was deposited around ca. 2.1 Ga.

3. Materials and methods

The Huaziyu magnesite deposit has two main magnesite ore bodies hosted within Mg-rich carbonates of the uppermost Member 3 in the Dashiqiao Formation (Fig. 1b). Both ore bodies have similar geological features. We focused on the upper magnesite ore body in this study (Fig. 1b). The base of this magnesite ore body comprises <10 m of dolomitic marble that is overlain by about 200 m of magnesite that is stratiform and conformable with the host rocks. A carbon-rich magnesite ore bed several meters thick is also observed in the middle of this magnesite ore body. The magnesite ore body is generally overlain by dolomitic marble and phyllite.

A range of textures in the magnesite ores and surrounding dolomitic marbles were observed in the field, including primary sedimentary structures, diagenetic fabrics, and recrystallization textures. Major sedimentary features include mud cracks and hail impressions beneath magnesite orebodies, horizontal bedding, and stromatolites in the magnesite ores (Fig. 2; Zhang, 1988). Diagenetic fabrics are represented by the appearance of diagenetic magnesite crystals in sedimentary magnesite and slump folds of diagenetic magnesite (Zhang, 1988). Nearly all of the magnesite ores in the Huaziyu deposit are characterized by intense recrystallization (Fig. 2). In addition to the two main magnesite orebodies, many smaller magnesite layers <15 m thick are hosted in dolomitic marbles and siliceous dolomitic marbles. These features of the Huaziyu magnesite

deposit are also typical of other giant strata-bound magnesite deposits (Jiang et al., 2004; Luo and Wang, 1989, 1990; Zhang, 1988).

Magnesite ore samples (M1 to M20) were collected from the Huaziyu magnesite deposit (Fig. 1). One dolomitic marble was also obtained from the footwall of the deposit (M21). For comparison, several thinner magnesite ores (M31, M32, M35, M36) and dolomitic marbles (C02, C03, C04, C06) were collected from Member 3 of the Dashiqiao Formation near Chenjiacun, which is about 14 km southwest of the Huaziyu deposit.

Rocks or ores were collected from surface outcrop that lacked obvious evidence for weathering. Samples were powdered in an agate mortar for bulk mineralogical and chemical analysis. The mineralogical compositions of all samples were determined by X-ray diffraction (XRD) at the Institute of Mineral Resources, Chinese Academy of Geological Sciences (CAGS). Major element concentrations were measured using X-ray fluorescence (XRF) spectroscopy at the Australian Laboratory Services Company. Each powdered sample was fused with a lithium metaborate-lithium tetraborate flux containing an oxidizing agent (lithium nitrate), and then poured into a platinum mound for analysis. The analytical reproducibility is generally within 5% for major oxides based on analysis of rock standards and duplicate samples. Loss on ignition (LOI) was measured by heating 1 g of sample powder at 1100°C for 1 h.

Trace element concentrations were measured by inductively coupled plasma mass spectrometry (ICP-MS, Finnigan MAT Element) at the Institute of Geochemistry, Chinese Academy of Sciences. About 100 mg of whole rock powder was digested by a mixture of concentrated HNO_3 and HCl in screw-top PTFE-lined stainless steel bombs at 190°C. Details regarding Q-ICP-MS analysis were described previously by Liang et al.

(2000). The analytical precision is generally better than 10% for all elements based on analysis of rock standards and duplicate samples.

Carbon and oxygen isotope compositions were measured using a Finnigan MAT 253 mass spectrometer coupled with a Thermo Finnigan GasBench II system at the Institute of Mineral Resources, CAGS. Carbonate micro-samples were loaded manually into 12 ml round-bottomed borosilicate Exetainers. A total of 88 Exetainers, including 18 aliquots of four national calcite standards (GBW04405, GBW04406, GBW04416, and GBW04417) are routinely analyzed during a single analytical session. The Exetainers are automatically flushed with grade 5 helium (flow rate of 100 ml/min) by penetrating the septa using a double-hole needle. Subsequently, four to six drops of phosphoric acid were added to each sample, which were then placed on an aluminum tray heated to 72°C for 4 h (dolomite) or 24 h (magnesite). The emitted CO_2 was separated from other volatile components using a gas chromatographic column heated to 72°C, and then passed into the mass spectrometer through an open split (see Spötl and Vennemann, 2003 for further details). The oxygen isotope fractionation factors of 1.008636, 1.009861, and 1.010022 at 72°C were applied for calcite, dolomite, and magnesite during the formation of CO_2 from carbonate by phosphoric acid reaction, respectively (Rosenbaum and Sheppard, 1986; Sharma et al., 2002). The $\delta^{13}C$ and $\delta^{18}O$ data are reported as per mil deviations relative to V-PDB. Based on reproducibility of the 18 calcite standards analyzed per run, the external precision of $\delta^{13}C$ and $\delta^{18}O$ is better than 0.1‰ (2σ).

Magnesium isotope analysis was carried out at the Laboratory of Isotope Geology, Institute of Geology, CAGS. About 10 to 50 mg of whole rock powder (depended on the Mg content) was digested by a mixture of concentrated HNO_3 and HCl (carbonate) or

HNO_3, HCl, and HF (basalt) in a clean room. Magnesium was separated by a two-stage column procedure using Bio-Rad AG50W-X12 resin (200-400 mesh) and eluted with HCl (Chang et al., 2003; Li et al., 2008). For the first stage, the resin bed was first washed 3 times with 3 ml of 0.5 M HF and ultrapure water, and then conditioned with 2.5 ml of 2 M HCl. The sample was then loaded in 0.3 ml of 2 M HCl. After washing with 1 ml of 2 M HCl, the sample was eluted by 6 ml of 2 M HCl. Before the second column, the eluted solution from the first column was dried down and re-dissolved with 0.4 M HCl. After conditioning the columns with 0.4 M HCl and sample loading, 12 ml of 0.4 M HCl was used to wash the resin. Magnesium was then collected by 6 ml of 6 M HCl. During column chemistry, one basaltic standard (BCR-2) was processed with each batch of unknown samples.

Magnesium isotope ratios were measured on a Nu Plasma HR-MC-ICP-MS (high-resolution multi-collector inductively coupled plasma mass spectrometer) instrument operating in high-resolution mode and using a sample-standard bracketing (SSB) approach to correct for instrumental mass fractionation. Samples are introduced into the mass spectrometer in 0.3 M HNO_3 using a DSN 100 desolvating nebulizer with Mg concentrations of about 1 μg ml^{-1}, where sample and standard solution concentrations are matched to within 10%. Data are acquired in blocks of 10 ratios with 10 s integration times, and background measurements are taken prior to each data block. The control system of the instrument is based on the Linux system, similar to the Nu Plasma HR-MC-ICP-MS at the University of Oxford (Belshaw et al., 2000). All Mg isotope results are reported relative to the DSM3 standard, and are expressed as:

$$\delta^{i}\mathrm{Mg} = [(^{i}\mathrm{Mg}/^{24}\mathrm{Mg})_{\mathrm{sample}}/(^{i}\mathrm{Mg}/^{24}\mathrm{Mg})_{\mathrm{DSM3}}-1]\times 1000\,,\ i = 25 \text{ or } 26.$$

The long-term external reproducibility of $\delta^{26}Mg$ and $\delta^{25}Mg$, based on repeated analyses of in-house standard solution CAGSMg2 relative to CAGSMg1, was 0.12‰ and 0.07‰, respectively (2SD, n = 91 in one year, see Inline Supplementary Fig. A.1). The $\delta^{26}Mg$ value of the CAGSMg2 solution relative to DSM3 was –0.37 ± 0.12‰ (2SD, n = 57 in one year, see Inline Supplementary Fig. A.2). The $\delta^{26}Mg$ value of DSM3 (measured against itself) was determined to be –0.06 ± 0.08‰ (2SD, n = 10). During the course of this study, the $\delta^{26}Mg$ value of basalt standard BCR-2 relative to DSM3 was –0.20 ± 0.08‰ (2SD, n = 3), which is identical to previously published values (Tipper et al., 2008).

4. Results

4.1 Mineralogy and major elements

Most of the magnesite ores are white, light pink, or steel grey. Significant recrystallization of magnesite is observed in the Huaziyu deposit (Fig. 2). The mineralogy of the ores is dominated by magnesite (>94%, with variable grain size and crystalloblastic texture) with only small amounts of quartz, dolomite, clinochlore, and talc. Dolomitic marble contains primarily dolomite and subordinate magnesite, quartz, and clinochlore. Quartz, carbonate, and clinochlore are preserved as a vein in one magnesite ore (M34) from the Dashiqiao Formation near Chenjiacun. The mineral compositions from the magnesite ores and dolomitic marbles are summarized in Inline Supplementary Fig. A.3 and Inline Supplementary Table A.1.

The major element compositions of the magnesite ores and dolomitic marbles are presented in Inline Supplementary Table A.2 and Fig. 3. For the magnesite ores, MgO and LOI are the dominant components, ranging from 40.80% to 47.50% (mean = 46.31 ±

3.08%, 2SD, n = 24) and 47.82% to 52.08% (mean = 51.22 ± 2.20%, 2SD, n = 24), respectively. The CaO content ranges from 0.21% to 2.50% (mean = 0.59 ± 0.92%, 2SD, n = 23), except for one dolomitic magnesite (M15; 7.61%). The Sr concentrations range between 0.60 and 9.16 mg/kg, except for the dolomitic magnesite (M15; 289 mg/kg). The SiO_2 content of the magnesite ores is lower than 1%, except for five magnesite samples (up to 8.24%). The Al_2O_3 (<0.64%), $Fe_2O_{3\ total}$ (<0.77%), and MnO (<0.06%) contents are low.

For dolomitic marbles, the MgO and CaO contents range from 17.40% to 21.60%, and from 26.20% to 30.40%, respectively. The SiO_2 and Al_2O_3 contents are 0.28-1.32% and 0.01-0.57%, respectively, except for one dolomitic marble (M21) that has high values of 12.10% and 2.57%, respectively. The $Fe_2O_{3\ total}$ (<1.42%) and MnO (<0.08%) contents are low.

4.2 Rare earth elements

The concentrations and patterns of REY (REE + Y) are presented in Inline Supplementary Table A.3 and Fig. 4, respectively. The REY data for the magnesite ores and dolomitic marbles are normalized relative to Post-Archean Australian Shale (PAAS, McLennan, 1989). Slightly positive Eu_{SN} anomalies are observed in both magnesite ores and dolomitic marbles (Fig. 4). The REY pattern of the magnesite ores from the Huaziyu deposit can be divided into two groups. One group has a flat to slightly medium (M)REE-enriched REY pattern with a low ΣREE concentration. This REY pattern is similar to that exhibited by dolomitic marbles from the Dashiqiao Formation and dolostones from the Paleoproterozoic Guanmenshan Group of NE China (Tang et al., 2013a). The other group

has a moderately LREE-depleted and slightly MREE-enriched pattern with a low ΣREE concentration.

4.3 Carbon and oxygen isotopes

The $\delta^{13}C$ and $\delta^{18}O$ values of the magnesite ores and dolomitic marbles are presented in Table 1 and Fig. 5. The magnesite ores and dolomitic marbles have a narrow range of $\delta^{13}C$ values from –0.42‰ to 1.17‰, which fall within the range of $\delta^{13}C$ observed in metasomatic magnesite from Australia and the eastern Alps (Aharon, 1988; Zadeh et al., 2015), but are more homogeneous. By contrast, the $\delta^{13}C$ values of the magnesite ores and dolomitic marbles analyzed in our study are generally higher than magnesite associated with ultramafic rocks (Fallick et al., 1991) and lower than Paleoproterozoic magnesite deposited in a playa or sabkha environment at the time of the Lomagundi Event (Melezhik et al., 2001).

The $\delta^{18}O$ values of the magnesite ores and dolomitic marbles range from –22.3‰ to –11.3‰, significantly lower than sabkha carbonate and salt lake magnesite deposited during the Holocene (Mees and Keppens, 2013) as well as Paleoproterozoic magnesites deposited in an evaporative environment (Melezhik et al., 2001). By contrast, the $\delta^{18}O$ values of the magnesite ores and dolomitic marbles are similar to metasomatic magnesite from Australia and the Eastern Alps (Aharon, 1988; Zedef et al., 2000).

4.4 Magnesium isotopes

The $\delta^{26}Mg$ values of all magnesite ores analyzed in this study range from –1.53‰ to –0.49‰ (mean = –0.87 ± 0.50‰, 2SD, n=24) (Table 1 and Fig. 6). The $\delta^{26}Mg$ values of

the magnesite and dolomitic marbles from Member 3 of the Dashiqiao Formation near Chenjiacun cluster in a narrow range from –1.21‰ to –1.04‰ (mean = –1.14 ± 0.15‰, 2SD, n=4) and from –1.48‰ to –1.07‰ (mean = –1.22 ± 0.35‰, 2SD, n=4), respectively. By comparison, most magnesite ores from the Huaziyu deposit have a narrow range of slightly more positive δ^{26}Mg values, typically between –0.95‰ and –0.49‰ (mean = –0.75 ± 0.26‰, 2SD, n=18). However, there are two highly negative δ^{26}Mg values in the Huaziyu deposit (M13 = –1.53‰ and M15 = –1.26‰). Sample M13 (magnesite ore) is not significantly different from other magnesite ores with respect to major and trace element concentrations, but sample M15 (dolomitic magnesite ore) has higher Ca and Sr concentrations. Sample M21 from the footwall of the Huaziyu magnesite deposit is a dolomitic marble and has a δ^{26}Mg value of –0.88‰, similar to the δ^{26}Mg values of the Huaziyu magnesite ores. However, sample M21 has significantly higher concentrations of Al, Fe, and Sc that point to an appreciable terrigenous component (with higher δ^{26}Mg) in this sample.

5. Interpretation and Discussion

The new Mg isotope dataset is the first for magnesites from giant strata-bound magnesite deposits. A notable feature of most Huaziyu magnesite ores is their higher δ^{26}Mg values (–0.75 ± 0.26‰, n=18) compared with most Proterozoic dolostones (Huang et al., 2015; Liu et al., 2014; Pokrovsky et al., 2011). Magnesium isotope compositions in bulk magnesite ores may not be significantly altered by regional prograde metamorphic dehydration, recrystallization, early diagenesis, and low-grade metamorphism (e.g., Geske et al., 2012; Higgins and Schrag, 2012; Wang et al., 2014, 2015), but it is possible

that fluids metasomatism/dolomitization could produce Mg isotope fractionation (e.g., Geske et al., 2015a; Walter et al., 2015). The C and O isotope compositions of the magnesite ores are similar to metasomatic magnesite from other localities, suggesting alteration of C and O isotope signatures during metasomatism. During recrystallization, the REY signatures of bulk magnesite ores may be affected by the presence of clay minerals, which contain significantly higher concentrations of REY compared with carbonates. Hence, caution is required when using these tracers (C, O isotopes and REY) to explain the magnesite formation. Below, we evaluate hydrothermal fluid metasomatism versus evaporative sedimentation plus brine diagenesis as mechanisms for producing the Huaziyu magnesite ores.

5.1 Hydrothermal metasomatism

One possible explanation for the formation of the Huaziyu magnesite ores is that hydrothermal metasomatism of carbonate rocks by Mg-rich fluids was the key factor responsible for magnesite formation (Luo and Wang, 1989, 1990). Two sources are possible: 1) a regional hydrothermal fluid that leached Mg from igneous, sedimentary, and metamorphic rocks, or 2) a local hydrothermal fluid that acquired most of its Mg from the immediately surrounding Mg-rich carbonates.

The scenario of regional hydrothermal fluid replacement is not consistent with the major and trace element geochemistry of the magnesite ores. Assuming a typical hydrothermal fluid chemically interacting on a regional scale with igneous and sedimentary rocks, the replacement of the carbonate precursor should lead to the formation of magnesite ores with a high Fe content (e.g., the $Fe_2O_{3\ total}$ content ranges

from 2.00% to 3.71% in metasomatic magnesite ores; Henjes-Kunst et al., 2014). A high Fe content in magnesite ores would result from the ion exchange between Fe^{2+} and Mg^{2+} (which have similar ionic radii) during hydrothermal replacement of the carbonate precursor (Bau et al., 1996). In addition, the originally low ΣREE of the carbonate precursor would be significantly affected by interaction with a hydrothermal fluid containing high ΣREE concentrations. However, the generally low contents of both Fe_2O_3 and ΣREE, as well as low contents of other important chemical constituents in hydrothermal fluids (e.g., MnO, Sr) are not consistent with formation of the magnesite ores via metasomatic processes involving an Fe-rich hydrothermal fluid.

Another possible replacement mechanism involves localized leaching of Mg by fluids from the surrounding Mg-rich Member 3 carbonates followed by replacement of the carbonate precursor by magnesite. The average $\delta^{26}Mg$ value of the dolomitic marble from Member 3 of the Dashiqiao Formation is –1.14 ± 0.15‰ (2SD, n = 4). Local dissolution of Member 3 carbonates should result in the fluid inheriting the Mg isotope composition of the carbonates if such rocks are the dominant source of Mg to the fluid. Homogenization temperatures of fluid inclusions in magnesite suggests that magnesite recrystallization occurred at 280-300°C (Chen et al., 2002). Even at 300°C, the Mg isotope fractionation between magnesite and fluid ($\Delta^{26}Mg_{magnesite\text{-}fluid}$) is still about –0.5‰ (estimated from Pearce et al., 2012). Hence, if most of the Mg was derived from the surrounding Mg-rich carbonates, then the magnesite ores produced by metasomatic replacement of the carbonate precursor should have $\delta^{26}Mg$ values that are lighter than the dolomitic marbles of Member 3. However, the $\delta^{26}Mg$ values of most of the magnesite ores are significantly heavier than the dolomitic marbles of Member 3, indicating that the

metasomatic fluid probably did not derive all of its Mg from the surrounding Mg-rich carbonates.

5.2 Evaporative sedimentation and brine diagenesis

Rather than hydrothermal metasomatism, an alternative hypothesis is evaporative sedimentation in a semi-closed system (e.g., a lagoon) (Chen et al., 2002; Zhang, 1988). The high atmospheric CO_2 level and high seawater alkalinity (e.g., Grotzinger and Kasting, 1993; Kaufman and Xiao, 2003; Ohmoto et al., 2004; Sheldon, 2006), and widespread stromatolites suggesting abundant microbial activity (Grotzinger and Knoll, 1999) would favor syn-sedimentary and diagenetic dolostone and magnesite formation in the Paleoproterozoic, consistent with the abundant dolomitic marbles and magnesite deposits in Member 3 of the Dashiqiao Formation, as well as stromatolites in the magnesite ores (Zhang, 1988).

Two sedimentary processes are possible for magnesite formation: 1) direct precipitation from evaporating seawater, or 2) magnesitization during brine diagenesis, which is described as that a diagenetic Mg-rich brine altered a Mg-rich carbonate precursor to magnesite, similar to dolomitization. The magnesite ores (δ^{26}Mg: –0.75 ± 0.26‰) and Member 3 magnesite (δ^{26}Mg: –1.14 ± 0.15‰) may have directly precipitated from highly evaporated seawater and less evaporated seawater, respectively. In this scenario, the δ^{26}Mg values of the local evaporating seawater and contemporaneous open ocean seawater should be ~1.2‰ and ~0.8‰, respectively, based on the magnesite-fluid fractionation factor of about –2‰ at 50°C (estimated from Pearce et al., 2012). Limited δ^{26}Mg variations have been inferred for Cenozoic seawater, despite the factor of four

variation in the seawater Mg/Ca ratios (Higgins and Schrag, 2015). However, it is impossible to deduce the δ^{26}Mg values of Paleoproterozoic seawater. In light of these observations, we cannot totally exclude the hypothesis of direct precipitation of magnesite from evaporating seawater based on the Mg isotope data. If the magnesite directly precipitated from evaporating seawater, then Paleoproterozoic seawater may have had much heavier δ^{26}Mg values (~0.8‰) than modern seawater (–0.82‰).

Another possible sedimentary process is magnesitization during brine diagenesis which would obviate the need to invoke high Paleoproterozoic seawater δ^{26}Mg values (~0.8‰). During the magnesitization, sediment pore fluids could be recognized as brine, and the magnesite would have formed by a chemical reaction between the brine and carbonate precursor, similar to the dolomitization. Due to incomplete exchange between sediment pore fluids and overlying brine, magnesites formed by the brine diagenesis would thus have higher δ^{26}Mg values than the magnesite which precipitated directly from the same brine.

Other potential factors likely influenced the δ^{26}Mg values of the magnesite ores during the magnesitization, including: 1) the δ^{26}Mg values of the brine, 2) Mg concentration of the brine, 3) rate of magnesite formation, 4) temperature, and 5) alkalinity and pH. The first three parameters are related to the brine composition and should be positively correlated with the δ^{26}Mg values of the magnesite ores. Rayleigh fractionation during sedimentary carbonate precipitation results in the δ^{26}Mg of the remaining water in the lagoon becoming enriched in the heavier Mg isotopes as lighter Mg isotopes are preferentially removed into carbonate. A similar process is observed in modern alkaline lakes, where the δ^{26}Mg of the lake water (~0.1‰) is significantly heavier

than the incoming spring/groundwater (–1.40‰ to –0.80‰) (Shirokova et al., 2013). Moreover, a higher rate of magnesite formation would lead to a heavier δ^{26}Mg value for the magnesite because of kinetic isotope fractionation (Immenhauser et al., 2010; Mavromatis et al., 2014). Higher Mg concentrations in the brine compared with contemporaneous seawater may result in a higher rate of magnesite formation during magnesitization, thus resulting in heavier δ^{26}Mg values for magnesite.

The effect of temperature is more difficult to evaluate. Higher temperatures promote seawater Mg^{2+} diffusion into the sediment during magnesitization. In contrast, a higher temperature would decrease the magnitude of Mg isotope fractionation between the carbonate and fluid, which is further supported by simulation experiments. In such experiments, a negative correlation between the temperature and magnitude of Mg isotope fractionation was observed in dolomite (Li et al., 2015) and magnesite (Pearce et al., 2012), suggesting gradients of 0.011‰/°C for dolomite and 0.014‰/°C for magnesite. The minor effect on δ^{26}Mg values of the diagenetic magnesite and limited temperature variation in the semi-closed system together suggest that temperature is not the key parameter controlling magnesite δ^{26}Mg during magnesitization.

In addition, other factors such as the greater alkalinity and possibly different pH (a consequence of higher atmospheric CO_2 partial pressures) of Paleoproterozoic seawater versus modern seawater (Grotzinger and Kasting, 1993; Kaufman and Xiao, 2003; Ohmoto et al., 2004; Sheldon, 2006) may have influenced the magnitude of Mg isotope fractionation during magnesite precipitation or initial precipitated mineral type during magnesitization. Evaluation of the effects of different physicochemical conditions on Mg isotope fractionation during magnesitization requires additional experimental studies.

The abundant dolostones from the Mesoproterozoic Wumishan Formation (3300 m thick) of North China have δ^{26}Mg values ranging from –1.72‰ to –1.35‰ (–1.51 ± 0.21‰, n=27), suggesting that a narrow range of low δ^{26}Mg in dolostones may originate from modification of the original carbonate sediments by diagenetic fluids derived from a seawater source (Huang et al., 2015). Similarly, the narrow range of heavier δ^{26}Mg values for the magnesite ores (–0.75 ± 0.26‰, n=18) implies that magnesite formation involved a diagenetic brine with heavier δ^{26}Mg values and higher Mg concentrations than contemporaneous seawater at the bottom of the lagoon. In addition, the geochemical characteristics of the brine (i.e., Mg-rich, Fe-poor, and REE-poor) are consistent with formation of nearly pure magnesite ores (as inferred from mineralogical observations) via diagenetic alteration of the carbonate precursor (Jiang et al., 2004). Hence, we suggest that Mg-rich brines accumulating in the bottom of the lagoon penetrated into carbonate sediments and altered the underlying carbonate precursor to form magnesite during diagenesis.

The hypothesis of brine diagenesis is consistent with the general slightly increasing trend in the δ^{26}Mg of the Huaziyu magnesite ores upsection (Fig. 6c). This trend could be explained by a gradual increase of the brine concentration and δ^{26}Mg values in the semi-closed evaporative system, with some reversals to lower δ^{26}Mg attributed to periodic incursions of seawater (with lower δ^{26}Mg values than the brine) into the basin.

Sabkha dolomites have variable δ^{26}Mg (–1.09‰ to –0.38‰; Geske et al., 2015b) that covers the δ^{26}Mg range of our magnesite ores. However, the supply of Mg is limited during sabkha formation, whereas an abundant Mg supply is required for formation of the strata-bound Huaziyu magnesite deposit. Hence, the deposit probably did not form in a

sabkha setting. Therefore, the carbonate precursor and the strata-bound magnesite deposits may have formed during evaporative sedimentation and brine diagenesis, respectively.

5.3 A genetic process for the formation of Paleoproterozoic magnesite deposits

The occurrence of calcium sulfate minerals with high $\delta^{34}S$ (~25‰) in the magnesite deposits (Chen et al., 2002) and the high $\delta^{11}B$ (~11‰) of the magnesite ores (Hu, 2014) both point to the precipitation of the original Mg-rich carbonate sediments in an evaporative environment. By contrast, the Fe concentration of the magnesite ores as well as REY and other elements cannot be explained by metasomatism via interaction with an Fe-rich regional hydrothermal fluid. The largely homogeneous and heavy Mg isotope compositions, and the carbon and oxygen isotope compositions of the magnesite ores suggest that both evaporative sedimentation and brine diagenesis played a critical role in the formation of the Huaziyu magnesite ores.

During seawater evaporation in a lagoon, lighter Mg isotopes are preferentially incorporated into the precursor Mg-rich carbonate sediments during precipitation, leaving the remaining seawater enriched in heavier Mg isotopes. Subsequently, seawater diagenesis likely formed dolomite and a limited amount of magnesite (e.g., magnesite and dolomitic marbles in Member 3 of the Dashiqiao Formation). Formation of large quantities of magnesite would be limited under relatively open-system conditions. When semi-closed conditions occurred, significant evaporation of seawater in the lagoon to form a Mg-rich brine, together with brine diagenesis of the Mg-rich carbonate precursor enabled the formation of abundant magnesite. The more positive $\delta^{26}Mg$ values of most

magnesite ores (–0.75 ± 0.26‰) from the Huaziyu deposit compared with the magnesites (–1.14 ± 0.15‰) and dolomitic marbles (–1.22 ± 0.35‰) from Member 3 of the Dashiqiao Formation can thus be explained in the context of different Mg sources (concentrated brine versus slightly evolved seawater, respectively). In brief, all of the geological and geochemical features of the magnesites and dolomitic marbles of the Dashiqiao Formation can be explained by the hypothesis of evaporative sedimentation plus brine diagenesis.

Hence, the combination of element concentrations and C, O, and Mg isotope data from the Huaziyu deposit sheds new insight on the formation mechanism of the giant strata-bound magnesite deposits in NE China. Initially, the local Paleoproterozoic seawater may have had a high Mg/Ca ratio relative to modern seawater due to the greater proportion of Archean Mg-rich ultramafic and mafic continental rocks exposed to weathering (e.g., Dhuime et al., 2015). The lower abundance of exposed ultramafic and mafic rocks on land during the Phanerozoic may be a key reason for the lack of giant strata-bound magnesite deposits in Phanerozoic sedimentary strata. In the region where the giant strata-bound magnesite deposits formed, Mg-rich carbonate precipitation first occurred in a marginal restricted marine environment, such as a lagoon. Evaporation and carbonate (including calcium sulfate) precipitation would have led to a significant increase in the Mg concentration of the lagoon seawater such that Mg-rich brines were produced. Subsequently, abundant magnesite was formed during brine diagenesis. The giant strata-bound magnesite deposits were subsequently affected by recrystallization to form the coarsely crystalline and saddle magnesite during regional metamorphism at ~1.9 Ga (Zhao and Zhai, 2013). Further modification of the magnesite Mg isotope

compositions may not have occurred during regional metamorphism as there is no evidence for Mg isotope fractionation during prograde metamorphic dehydration (Wang et al., 2014).

6. Conclusions

We obtained the first Mg isotope data from the world's largest strata-bound magnesite deposit belt, hosted by the ca. 2.1 Ga Dashiqiao Formation in NE China. Based on Mg, O, and C isotope compositions, element concentrations, and geological features, we infer that the formation of the Huaziyu magnesite deposit was dominated by evaporative sedimentation and brine diagenesis. Abundant Mg-rich carbonate precipitated from seawater in a semi-closed evaporative environment such as a lagoon, thus forming the Mg-rich brine. Most magnesite formed by magnesitization during a Mg-rich brine diagenesis. Later, the magnesite was transformed into giant magnesite ores during regional metamorphism. Giant strata-bound magnesite deposits are absent in modern and most Phanerozoic sedimentary environments but occur predominantly in Precambrian strata possibly because Mg-rich seawater (from weathering of Mg-rich ultramafic and mafic rocks of Archean age) is a key requirement to generate magnesite, which in turn can produce highly Mg-rich brines via evaporation, thus enabling the formation of magnesite during brine diagenesis.

Acknowledgements

The authors acknowledge Bing Shen and Xue-lei Chu for discussion, Yong Li and Zhongbo He for field assistance, Biao Jin, Xuexian He and Nick S Belshaw for technical

assistance of Mg isotope measurements, and Albert Galy for providing the DSM3 standard solution. The paper benefited from detailed and insightful comments of Adrian Immenhauser and one anonymous reviewer, and efficient editing from Guochun Zhao. This work is financially supported by the National Natural Science Foundation of China (41203004) and MLR Public Benefit Research Foundation of China (201211074). Kendall acknowledges support from a NSERC Discovery Grant.

Appendix A. Supplementary material

References

Aharon, P., 1988. A stable-isotope study of magnesites from the Rum Jungle uranium field, Australia: implications for the origin of strata-bound massive magnesites. Chemical Geology 69, 127-145.

Alibo, D.S., Nozaki, Y., 1999. Rare earth elements in seawater: Particle association, shale-normalization, and Ce oxidation. Geochimica et Cosmochimica Acta 63, 363-372.

Azmy, K., Lavoie, D., Wang, Z., Brand, U., Al-Aasm, I., Jackson, S., Girard, I., 2013. Magnesium-isotope and REE compositions of Lower Ordovician carbonates from eastern Laurentia: implications for the origin of dolomites and limestones. Chemical Geology, 64-75.

Bau, M., Dulski, P., 1996. Distribution of yttrium and rare-earth elements in the Penge and Kuruman iron-formations, Transvaal Supergroup, South Africa. Precambrian Research 79, 37-55.

Bau, M., Dulski, P., 1999. Comparing yttrium and rare earths in hydrothermal fluids from the Mid-Atlantic Ridge: implications for Y and REE behaviour during near-vent mixing and for the Y/Ho ratio of Proterozoic seawater. Chemical Geology 155, 77-90.

Blättler, C.L., Miller, N.R., Higgins, J.A., 2015. Mg and Ca isotope signatures of authigenic dolomite in siliceous deep-sea sediments. Earth and Planetary Science Letters 419, 32-42.

Bekker, A., Holland, H., 2012. Oxygen overshoot and recovery during the early Paleoproterozoic. Earth and Planetary Science Letters 317, 295-304.

Bekker, A., Karhu, J.A., Kaufman, A.J., 2006. Carbon isotope record for the onset of the Lomagundi carbon isotope excursion in the Great Lakes area, North America. Precambrian Research 148, 145-180.

Belshaw, N., Zhu, X., Guo, Y., O'Nions, R., 2000. High precision measurement of iron isotopes by plasma source mass spectrometry. International Journal of Mass Spectrometry 197, 191-195.

Chang, V.T.C., Makishima, A., Belshaw, N.S., O'Nions, R.K., 2003. Purification of Mg from low-Mg biogenic carbonates for isotope ratio determination using multiple collector ICP-MS. J. Anal. At. Spectrom. 18, 296-301.

Chang, V.T.C., Williams, R., Makishima, A., Belshawl, N.S., O'Nions, R.K., 2004. Mg and Ca isotope fractionation during $CaCO_3$ biomineralisation. Biochemical and biophysical research communications 323, 79-85.

Chen, C., Lu, A., Cai, K., Zhai, Y., 2002. Sedimentary characteristics of Mg-rich carbonate formations and minerogenic fluids of magnesite and talc occurrences in

early Proterozoic in eastern Liaoning Province, China. Science in China Series B: Chemistry 45, 84-92.

Dhuime, B., Wuestefeld, A., Hawkesworth, C.J., 2015. Emergence of modern continental crust about 3 billion years ago. Nature Geoscience 8, 552-555.

Dong, Q., Feng, B., Li, X., 1996. The lithofacies and paleographical setting of Haicheng-Dashiqiao Super-large magnesite deposits, Liaoning Province. Journal of Changchun University of Earth Sciences 26(supp.), 69-73. (in Chinese with English abstract)

Douville, E., Bienvenu, P., Charlou, J.L., Donval, J.P., Fouquet, Y., Appriou, P., Gamo, T., 1999. Yttrium and rare earth elements in fluids from various deep-sea hydrothermal systems. Geochimica et Cosmochimica Acta 63, 627-643.

Fallick, A.E., Ilich, M., Russell, M.J., 1991. A stable isotope study of the magnesite deposits associated with the Alpine-type ultramafic rocks of Yugoslavia. Economic Geology 86, 847-861.

Feng, B., Zhu, G., Dong, Q., Zeng, Z., 1995. Geological characteristics and genesis of Haicheng – Dashiqiao superlarge magnesite deposits, eastern Liaoning province. Journal of Changchun university of Earth Sciences 25, 121-124. (in Chinese with English abstract)

Frank, T.D., Fielding, C.R., 2003. Marine origin for Precambrian, carbonate-hosted magnesite? Geology 31, 1101-1104.

Galy, A., Bar-Matthews, M., Halicz, L., O'Nions, R.K., 2002. Mg isotopic composition of carbonate: insight from speleothem formation. Earth and Planetary Science Letters 201, 105-115.

Geske, A., Goldstein, R., Mavromatis, V., Richter, D., Buhl, D., Kluge, T., John, C., Immenhauser, A., 2015a. The magnesium isotope (δ^{26}Mg) signature of dolomites. Geochimica et Cosmochimica Acta 149, 131-151.

Geske, A., Lokier, S., Dietzel, M., Richter, D.K., Buhl, D., Immenhauser, A., 2015b. Magnesium isotope composition of sabkha porewater and related (Sub-) Recent stoichiometric dolomites, Abu Dhabi (UAE). Chemical Geology 393-394, 112-124.

Grotzinger, J.P., Kasting, J.F., 1993. New constraints on Precambrian ocean composition. Journal of Geology 101, 235-243.

Grotzinger, J.P., Knoll, A.H., 1999. Stromatolites in Precambrian carbonates: evolutionary mileposts or environmental dipsticks? Annual Review of Earth and Planetary Sciences 27, 313-358.

Henjes-Kunst, F., Prochaska, W., Niedermayr, A., Sullivan, N., Baxter, E., 2014. Sm-Nd dating of hydrothermal carbonate formation: An example from the Breitenau magnesite deposit (Styria, Austria). Chemical Geology 387, 184-201.

Higgins, J., Schrag, D., 2012. Records of Neogene seawater chemistry and diagenesis in deep-sea carbonate sediments and pore fluids. Earth and Planetary Science Letters 357, 386-396.

Higgins, J.A., Schrag, D.P., 2015. The Mg isotopic composition of Cenozoic seawater – evidence for a link between Mg-clays, seawater Mg/Ca, and climate. Earth and Planetary Science Letters 416, 73-81.

Huang, K.-J., Shen, B., Lang, X.-G., Tang, W.-B., Peng, Y., Ke, S., Kaufman, A.J., Ma, H.-R., Li, F.-B., 2015. Magnesium isotopic compositions of the Mesoproterozoic

dolostones: Implications for Mg isotopic systematics of marine carbonates. Geochimica et Cosmochimica Acta 164, 333-351.

Hu, G.-Y., 2014, Marine Evaporative Genesis and Formation Age of Paleoproterozoic Borate Deposits, Eastern Liaoning Province: Constrains from Isotopic Geochemistry [Ph.D. thesis]: Chinese Academy of Geological Sciences, Beijing, 148. (in Chinese with English abstract)

Immenhauser, A., Buhl, D., Richter, D., Niedermayr, A., Riechelmann, D., Dietzel, M., Schulte, U., 2010. Magnesium-isotope fractionation during low-Mg calcite precipitation in a limestone cave-Field study and experiments. Geochimica et Cosmochimica Acta 74, 4346-4364.

Jiang, S., Chen, C., Chen, Y., Jiang, Y., Dai, B., Ni, P., 2004. Geochemistry and genetic model for the giant magnesite deposits in the eastern Liaoning province, China. Acta Petrologica Sinica 20, 765-772.

Kaufman, A.J., Xiao, S., 2003. High CO_2 levels in the Proterozoic atmosphere estimated from analyses of individual microfossils. Nature 425, 279-282.

Lavoie, D., Jackson, S., Girard, I., 2014. Magnesium isotopes in high-temperature saddle dolomite cements in the lower Paleozoic of Canada. Sedimentary Geology 305, 58-68.

Li, S. -Z., Zhu, X. -K., He, X., Yang, C., Zhao, X., Tang, S., 2008. Separation of Mg for isotope determination by MC- ICP- MS. Acta Petrological et Mineralogica 27, 449-456. (in Chinese with English abstract)

Li, W., Beard, B.L., Li, C., Xu, H., Johnson, C.M., 2015. Experimental calibration of Mg isotope fractionation between dolomite and aqueous solution and its geological

implications. Geochimica et Cosmochimica Acta 157, 164-181.

Liang, Q., Jing, H., Gregoire, D.C., 2000. Determination of trace elements in granites by inductively coupled plasma mass spectrometry. Talanta 51, 507-513.

Ling, M.X., Sedaghatpour, F., Teng, F.Z., Hays, P.D., Strauss, J., Sun, W., 2011. Homogeneous magnesium isotopic composition of seawater: an excellent geostandard for Mg isotope analysis. Rapid Communications in Mass Spectrometry 25, 2828-2836.

Liu, C., Wang, Z., Raub, T.D., Macdonald, F.A. and Evans, D.A. (2014) Neoproterozoic cap-dolostone deposition in stratified glacial meltwater plume. Earth and Planetary Science Letters 404, 22-32.

Luo, Y., Wang, Y., 1989. A preliminary study on the genesis of the Dashiqiao sparry magnesite deposits in the light of some geological features. Mineral Deposits 8, 71-84. (in Chinese with English abstract)

Luo, Y., Wang, Y., 1990. Geological and geochemical features of the ore from the Dashiqiao magnesite deposit. Mineral Deposits 9, 77-85. (in Chinese with English abstract)

Mavromatis, V., Gautier, Q., Bosc, O., Schott, J., 2013. Kinetics of Mg partition and Mg stable isotope fractionation during its incorporation in calcite. Geochimica et Cosmochimica Acta 114, 188-203.

Mavromatis, V., Meister, P., Oelkers, E.H., 2014. Using stable Mg isotopes to distinguish dolomite formation mechanisms: A case study from the Peru Margin. Chemical Geology 385, 84-91.

McLennan, S., 1989. Rare earth elements in sedimentary rocks; influence of provenance

and sedimentary processes. Reviews in Mineralogy and Geochemistry 21, 169-200.

Mees, F., Keppens, E., 2013. Stable isotope geochemistry of magnesite from Holocene salt lake deposits, Taoudenni, Mali. Geological Journal 48, 620-627.

Melezhik, V.A., Fallick, A.E., Medvedev, P.V., Makarikhin, V.V., 2001. Palaeoproterozoic magnesite: lithological and isotopic evidence for playa/sabkha environments. Sedimentology 48, 379-397.

Melezhik, V.A., Fallick, A.E., Rychanchik, D.V., Kuznetsov, A.B., 2005. Paleoproterozoic evaporites in Fennoscandia: implications for seawater sulphate, $\delta^{13}C$ excursions and the rise of atmospheric oxygen. Terra Nova 17, 141-148.

Ohmoto H., Watanabe, Y., Kumazawa, K., 2004. Evidence from massive siderite beds for a CO_2-rich atmosphere before ~1.8 billion years ago. Nature 429, 395-399.

Pearce, C.R., Saldi, G.D., Schott, J., Oelkers, E.H., 2012. Isotopic fractionation during congruent dissolution, precipitation and at equilibrium: Evidence from Mg isotopes. Geochimica et Cosmochimica Acta 92, 170-183.

Planavsky, N.J., Bekker, A., Hofmann, A., Owens, J.D., Lyons, T.W., 2012. Sulfur record of rising and falling marine oxygen and sulfate levels during the Lomagunid Event. Proceedings of the National Academy of Sciences USA 109, 18300-18305.

Pohl, W., 1990. Genesis of magnesite deposits—models and trends. Geologische Rundschau 79, 291-299.

Pokrovsky, B.G., Mavromatis, V. and Pokrovsky, O.S. (2011) Co-variation of Mg and C isotopes in late Precambrian carbonates of the Siberian Platform: A new tool for

tracing the change in weathering regime? Chemical Geology 290, 67-74.

Power, I.M., Wilson, S.A., Harrison, A.L., Dipple, G.M., Mccutcheon, J., Southam, G., Kenward, P.A., 2014. A depositional model for hydromagnesite–magnesite playas near Atlin, British Columbia, Canada. Sedimentology 61, 1701-1733.

Reuschel, M., Melezhik, V.A., Whitehouse, M.J., Lepland, A., Fallick, A.E., Strauss, H., 2012. Isotopic evidence for a sizable seawater sulfate reservoir at 2.1 Ga. Precambrian Research 192-195, 78-88.

Rosenbaum, J., Sheppard, S.M.F., 1986. An isotopic study of siderites, dolomites and ankerites at high temperatures. Geochimica et Cosmochimica Acta 50, 1147-1150.

Sharma, S.D., Patil, D.J., Gopalan, K., 2002. Temperature dependence of oxygen isotope fractionation of CO2 from magnesite-phosphoric acid reaction. Geochimica et Cosmochimica Acta 66, 589-593.

Schröder, S., Bekker, A., Beukes, N.J., Strauss, H., van Niekerk, H.S., 2008. Rise in seawater sulphate concentration associated with the Paleoproterozoic positive carbon isotope excursion: evidence from sulphate evaporites in the ~2.2-2.1 Gyr shallow-marine Lucknow Formation, South Africa. Terra Nova 20, 108-117.

Scott, C., Wing, B.A., Bekker, A., Planavsky, N.J., Medvedev, P., Bates, S.M., Yun, M., Lyons, T.W., 2014. Pyrite multiple-sulfur isotope evidence for rapid expansion and contraction of the early Paleoproterozoic seawater sulfate reservoir. Earth and Planetary Science Letters 389, 95-104.

Sheldon, N.D., 2006. Precambrian paleosols and atmospheric CO_2 levels. Precambrian Research 147, 148-155.

Shirokova, L.S., Mavromatis, V., Bundeleva, I.A., Pokrovsky, O.S., Bénézeth, P., Gérard,

E., Pearce, C.R., Oelkers, E.H., 2013. Using Mg isotopes to trace cyanobacterially mediated magnesium carbonate precipitation in alkaline lakes. Aquatic Geochemistry 19, 1-24.

Spötl, C., Vennemann, T.W., 2003. Continuous-flow isotope ratio mass spectrometric analysis of carbonate minerals. Rapid communications in mass spectrometry 17, 1004-1006.

Tang, H.-S., Chen, Y.-J., Wu, G., Lai, Y., 2011. Paleoproterozoic positive $\delta^{13}C$ excursion in the northeastern Sino-Korean craton: Evidence of the Lomagundi Event. Gondwana Research 19, 471-481.

Tang, H.-S., Chen, Y.-J., Santosh, M., Zhong, H., Yang, T., 2013a. REE geochemistry of carbonates from the Guanmenshan Formation, Liaohe Group, NE Sino-Korean Craton: Implications for seawater compositional change during the Great Oxidation Event. Precambrian Research 227, 316-336.

Tang, H.-S., Chen, Y.-J., Santosh, M., Zhong, H., Wu, G., Lai, Y., 2013b. C-O isotope geochemistry of the Dashiqiao magnesite belt, North China Craton: implications for the Great Oxidation Event and ore genesis. Geological Journal 48, 467-483.

Teng, F.-Z., Wadhwa, M., Helz, R.T., 2007. Investigation of magnesium isotope fractionation during basalt differentiation: implications for a chondritic composition of the terrestrial mantle. Earth and Planetary Science Letters 261, 84-92.

Tipper, E.T., Louvat, P., Capmas, F., Galy, A., Gaillardet, J., 2008. Accuracy of stable Mg and Ca isotope data obtained by MC-ICP-MS using the standard addition method. Chemical Geology 257, 65-75.

Wan, Y., Song, B., Liu, D., Wilde, S.A., Wu, J., Shi, Y., Yin, X., Zhou, H., 2006. SHRIMP U–Pb zircon geochronology of Palaeoproterozoic metasedimentary rocks in the North China Craton: Evidence for a major Late Palaeoproterozoic tectonothermal event. Precambrian Research 149, 249-271.

Wang, S.-J., Teng, F.-Z., Li, S.-G., Hong, J.-A., 2014. Magnesium isotopic systematics of mafic rocks during continental subduction. Geochimica et Cosmochimica Acta 143, 34-48.

Wang, S.-J., Teng, F.-Z., Bea, F., 2015. Magnesium isotopic systematics of metapelite in the deep crust and implications for granite petrogenesis. Geochemical Perspectives Letters 1, 75-83.

Walter, B.F., Immenhauser, A., Geske, A., Markl, G., 2015. Exploration of hydrothermal carbonate magnesium isotope signatures as tracers for continental fluid aquifers, Schwarzwald mining district, SW Germany. Chemical Geology 400, 87-105.

Warren, J., 2000. Dolomite: occurrence, evolution and economically important associations. Earth-Science Reviews 52, 1-81.

Zadeh, A.M.A., Ebner, F., Jiang, S.-Y., 2015. Mineralogical, geochemical, fluid inclusion and isotope study of Hohentauern/Sunk sparry magnesite deposit (Eastern Alps/Austria): implications for a metasomatic genetic model. Mineralogy and Petrology, 1-21.

Zedef, V., Russell, M.J., Fallick, A.E., Hall, A.J., 2000. Genesis of vein stockwork and sedimentary magnesite and hydromagnesite deposits in the ultramafic terranes of southwestern Turkey: A stable isotope study. Economic Geology 95, 429-445.

Zhang, Q., 1988. Early proterozoic tectonic styles and associated mineral deposits of the

North China Platform. Precambrian Research 39, 1-29.

Zhao, G., Zhai, M., 2013. Lithotectonic elements of Precambrian basement in the North China Craton: Review and tectonic implications. Gondwana Research 23, 1207-1240.

Figure captions

Figure 1. Sample location and stratigraphy of the Huaziyu magnesite deposit, modified from Zhang (1988).

Figure 2. Photos and photomicrographs of magnesite ores from the Huaziyu deposit in NE China. a. Huaziyu magnesite deposit; b. Magnesite ores and mafic dyke; c. Magnesite ores (stromatolite pseudomorph?) d. Pink recrystallized magnesite ores; e. Interbedded magnesite ores (white and black); f. Pure recrystallized magnesite ores; g. Photomicrograph of magnesite ores (polarized light); h. Photomicrograph of recrystallized magnesite ores (crossed-polarized light); i. Photomicrograph of magnesite ores (cross-polarized light). Abbreviations: Mgs = magnesite; Qtz = quartz; Tlc = Talc.

Figure 3. Major and trace element concentrations of the magnesite ores in the profile section from the Huaziyu deposit.

Figure 4. The REE + Y (REY) distribution pattern of magnesite ores and dolomitic marbles from the Dashiqiao Formation of NE China. Data sources: a from Tang et al. (2013a); b from Aharon (1988); Zadeh et al. (2015); c from Alibo and Nozaki (1999); d from Bau and Dulski (1999); e from Bau and Dulski (1996); f from Douville et al. (1999). PAAS = Post-Archean Australian Shale.

Figure 5. The $\delta^{13}C$ and $\delta^{18}O$ values of magnesite ores and dolomitic marbles from the Dashiqiao Formation of NE China as well as other marine carbonates (magnesite and

dolostone) and magnesites associated with ultramafic rocks, salt lakes, and metasomatism. Data sources: a from Mees and Keppens (2013); b from Fallick et al. (1991); c from Tang et al. (2011); d from Melezhik et al. (2001); e from Aharon (1988); f from Zadeh et al. (2015).

Figure 6. Magnesium isotopic composition of seawater, lake water, magnesite, limestone, and dolostone. a. Bar chart of Mg isotope compositions from the magnesites and dolomitic marbles analyzed for this study. b. Mg isotope composition of other carbonates and waters. The gray bar represents the bulk Earth composition from Teng et al. (2007). Data sources: *a* from Shirokova et al. (2013); *b* from Blättler et al. (2015); *c* from Geske et al. (2015a); *d* from Geske et al. (2012); Azmy et al. (2013); Geske et al. (2015b); *e* from Galy et al. (2002); Jacobson et al. (2010); Geske et al. (2012); Sun et al. (2012); Azmy et al. (2013); Lavoie et al. (2014); Geske et al. (2015); *f* from Galy et al. (2002); Immenhauser et al. (2010); Azmy et al. (2013); *g* from Ling et al. (2011). c. Geochemical profile of Mg isotope compositions of the magnesite ores from the Huaziyu deposit.

Table 1. Mg, C, and O isotope compositions measured in this study

Sample	Type	Schematic Sedimentary depth (m)	Location	δ^{26}Mg	2sd	δ^{25}Mg	2sd	δ^{13}C	δ^{18}O
M01	Magnesite	-10	HZY	-0.65	0.05	-0.31	0.01	0.70	-19.30
M02	Magnesite	-20	HZY	-0.49	0.08	-0.26	0.01	-0.26	-18.31
M03	Magnesite	-30	HZY	-0.67	0.09	-0.35	0.06	0.80	-18.87
M04	Magnesite	-40	HZY	-0.63	0.04	-0.31	0.04	N.D.	N.D.
M05	Magnesite	-50	HZY	-0.65	0.06	-0.34	0.00	0.69	-18.34
M06	Magnesite	-60	HZY	-0.85	0.14	-0.43	0.04	0.67	-18.41
M07	Magnesite	-70	HZY	-0.73	0.04	-0.36	0.06	0.81	-18.87
M08	Magnesite	-80	HZY	-0.74	0.03	-0.36	0.10	N.D.	N.D.
M09	Magnesite	-90	HZY	-0.76	0.12	-0.40	0.05	0.79	-19.10
M10	Magnesite	-100	HZY	-0.77	0.10	-0.39	0.04	N.D.	N.D.
M11	Magnesite	-110	HZY	-0.53	0.00	-0.26	0.04	0.76	-11.32
M12	Magnesite	-120	HZY	-0.88	0.04	-0.45	0.04	N.D.	N.D.
M13	Magnesite	-130	HZY	-1.53	0.11	-0.78	0.05	0.82	-16.92
M14	Magnesite	-140	HZY	-0.82	0.05	-0.42	0.03	N.D.	N.D.
M15	Dolomitic magnesite	-150	HZY	-1.26	0.09	-0.64	0.06	-0.42	-22.29
M16	Magnesite	-160	HZY	-0.89	0.06	-0.45	0.09	0.94	-17.21
M17	Magnesite	-170	HZY	-0.95	0.08	-0.48	0.05	1.17	-17.02
M18	Magnesite	-180	HZY	-0.88	0.12	-0.44	0.06	N.D.	N.D.
M19	Magnesite	-190	HZY	-0.85	0.03	-0.42	0.04	0.69	-16.84
M20	Magnesite	-200	HZY	-0.82	0.07	-0.41	0.05	N.D.	N.D.
M21	Dolomitic marble	-210	HZY	-0.88	0.00	-0.43	0.00	0.37	-16.14
M31	Magnesite		CJC	-1.14	0.06	-0.54	0.03	0.81	-15.96
M32	Magnesite		CJC	-1.04	0.13	-0.55	0.08	1.03	-16.00
M35	Magnesite		CJC	-1.21	0.00	-0.64	0.04	0.79	-16.00
M36	Magnesite		CJC	-1.18	0.00	-0.63	0.07	N.D.	N.D.
C02	Dolomitic marble		CJC	-1.14	0.04	-0.60	0.01	N.D.	N.D.
C03	Dolomitic marble		CJC	-1.07	0.13	-0.55	0.05	0.95	-12.55
C04	Dolomitic marble		CJC	-1.48	0.01	-0.77	0.02	N.D.	N.D.
C06	Dolomitic marble		CJC	-1.20	0.07	-0.63	0.06	0.62	-15.86

N.D., no data; HZY, Huaziyu deposit; CJC, Chenjiacun; 2SD, 2 times the standard deviation.

Magnesium, carbon and oxygen isotope results are reported as per mil deviations relative to the DSM3 and V-PDB standards, respectively.

Figure1

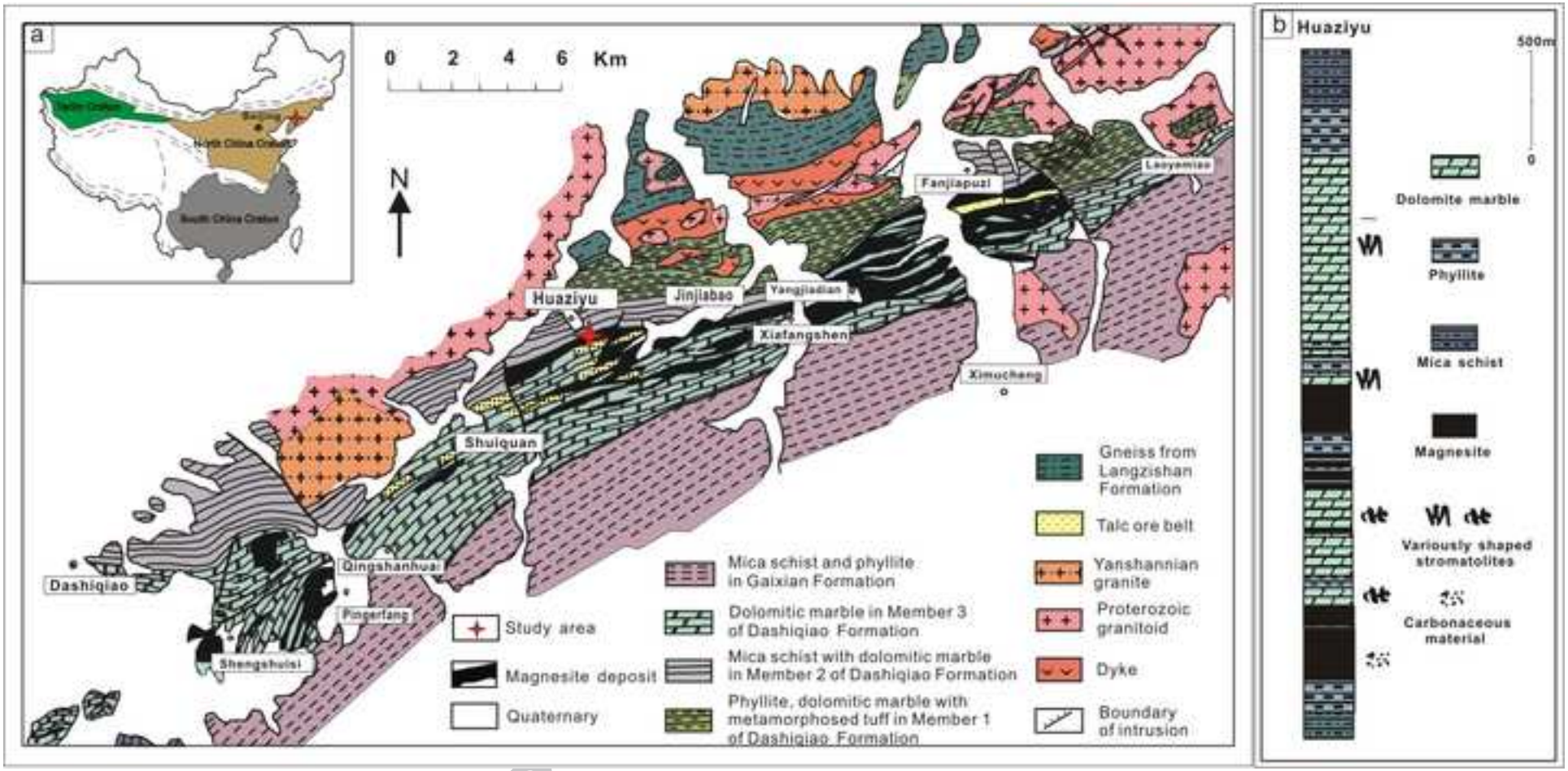

Figure2

Figure3

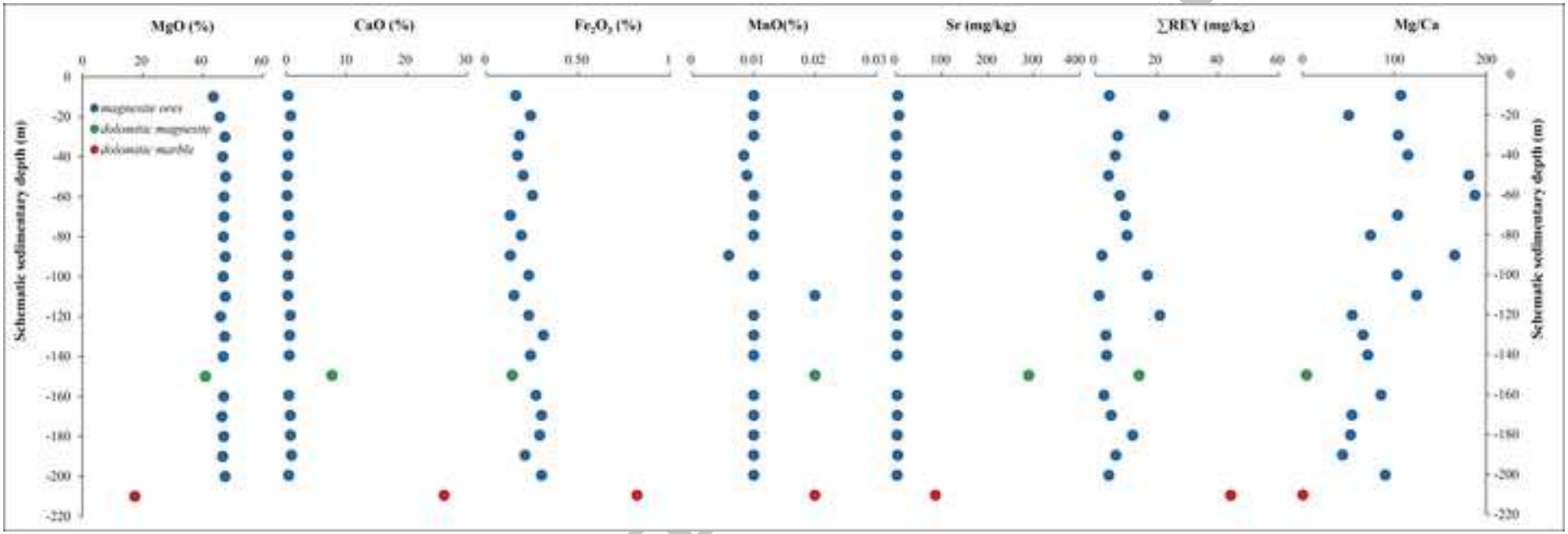

Figure4

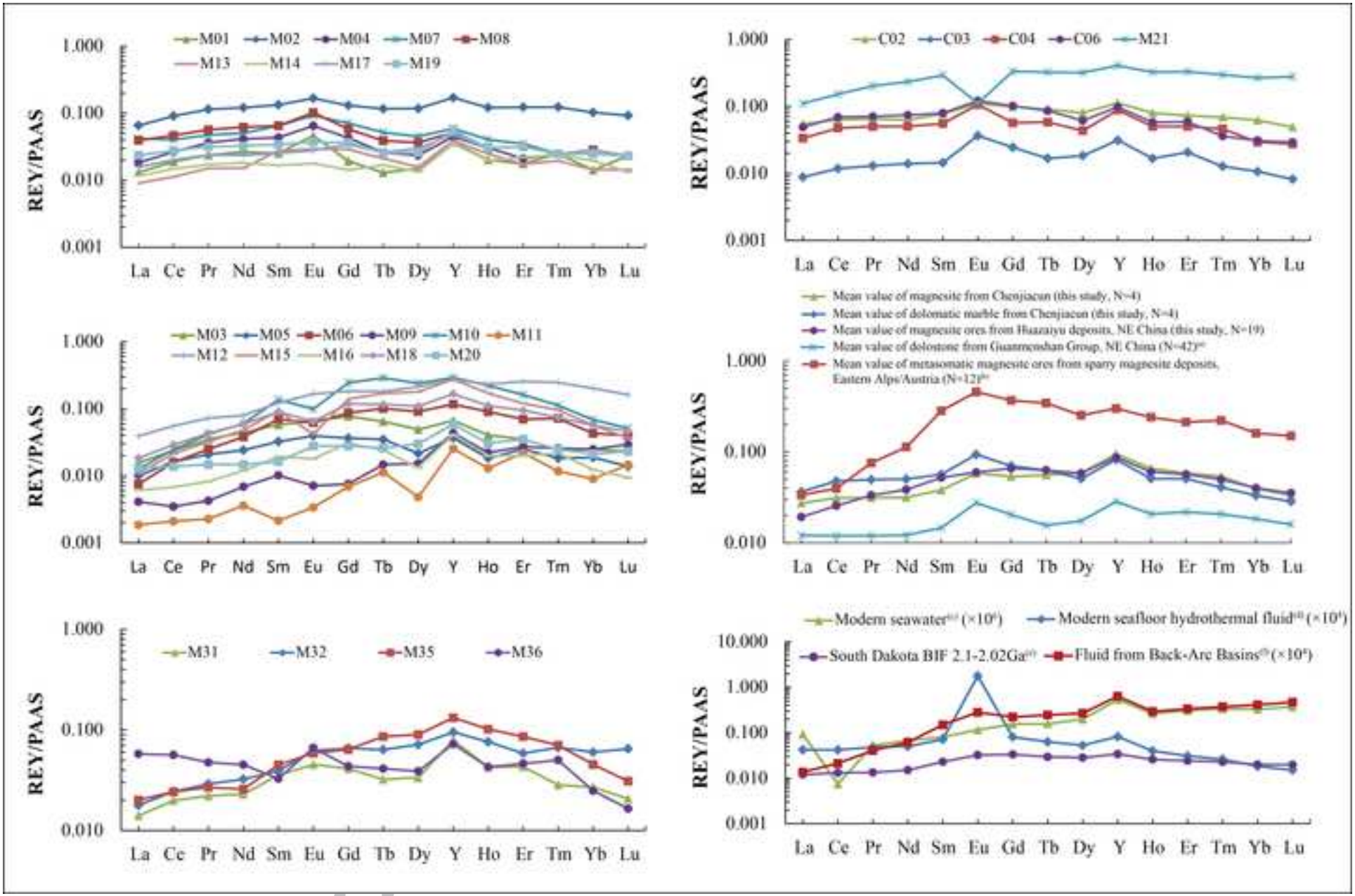

Figure5

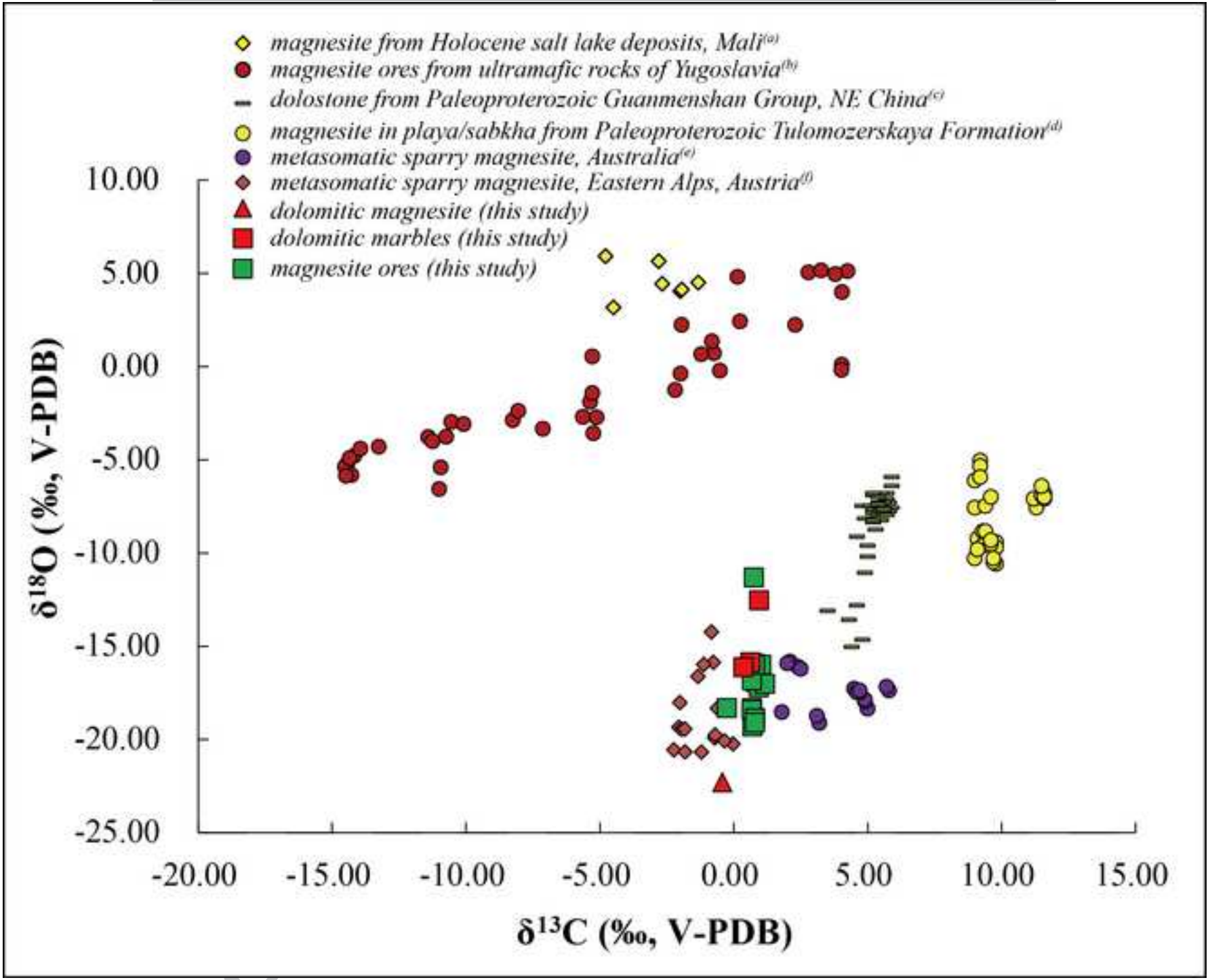

Figure6

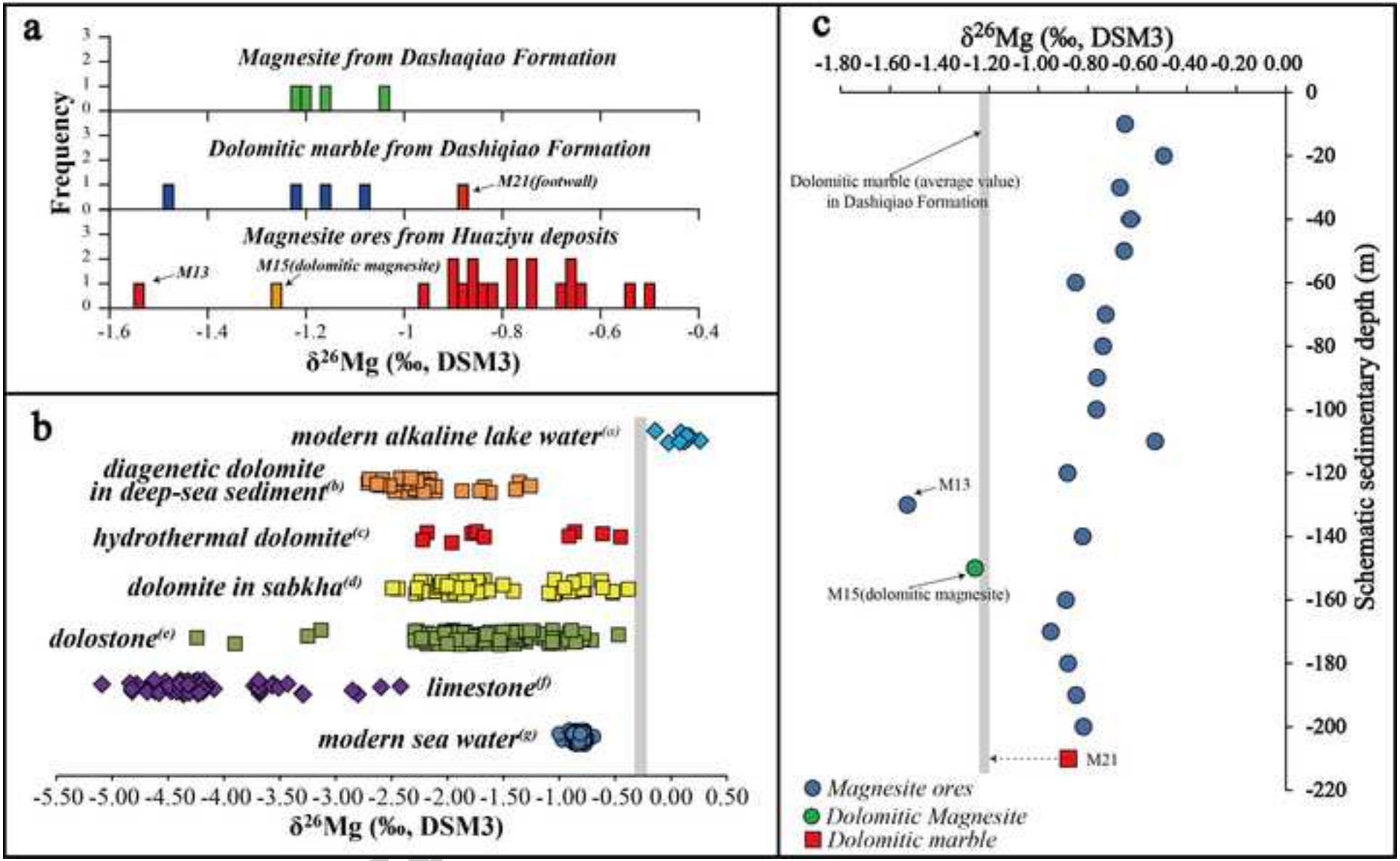

Highlights

- We obtained the first Mg isotope data from Paleoproterozoic magnesite deposits.
- The results rule out the possibility that the magnesites are of hydrothermal origin.
- The Mg isotope data can be explained by magnesitization during diagenesis.